Diffusion and interaction of prismatic dislocation loops simulated by stochastic discrete dislocation dynamics

Yang Li,[1,*] Max Boleininger,[2,†] Christian Robertson,[1,‡] Laurent Dupuy,[1,§] and Sergei L. Dudarev[2,‖]
[1]*DEN-Service de Recherches Métallurgiques Appliquées, CEA, Université Paris-Saclay, F-91191, Gif-sur-Yvette, France*
[2]*CCFE, Culham Science Centre, UK Atomic Energy Authority, Abingdon, Oxfordshire OX14 3DB, United Kingdom*

(Received 25 March 2019; published 23 July 2019)

Body-centered cubic metals and alloys irradiated by energetic particles form highly mobile prismatic dislocation loops with $a/2\langle 111\rangle$-type Burgers vectors. We show how to simulate thermal diffusion of prismatic loops using a discrete dislocation dynamics approach that explicitly includes the stochastic forces associated with ambient thermal fluctuations. We find that the interplay between stochastic thermal forces and internal degrees of freedom of loops, in particular the reorientation of the loop habit planes, strongly influences the observed loop dynamics. The loops exhibit three fundamental types of reactions: coalescence, repulsion, and confinement by elastic forces. The confinement reactions are highly sensitive to the internal degrees of freedom of the loops. Depending on the orientation of the loop habit planes, the barrier to enter an elastically confined bound state is lowered substantially, whereas the lifetime of the bound state increases by many orders of magnitude.

DOI: 10.1103/PhysRevMaterials.3.073805

I. INTRODUCTION

Metals exposed to irradiation develop a highly complex microstructure, involving a mixture of mobile and immobile defects of both interstitial and vacancy type. The defect and dislocation network develops under the effect of internal and external stresses, and temperature, generating its own fluctuating stress field. This leads to a variety of changes in mechanical properties, such as hardening and the loss of ductility, having a detrimental effect on the longevity of structural reactor components in a radiation environment.

Predicting the dynamics of evolution of microstructure is a major challenge to computer modeling because of the broad spectrum of activation energies characterizing defect and dislocation networks. Defect cluster migration barriers vary from meVs to eVs. The binding energy of elastically confined defect structures spans a similar range of energy scales [1], and the magnitude of elastic interaction depends on the size of defects and their spatial distribution. Simulating the temperature dependent dynamics of microstructure requires the treatment of intrinsic thermally activated Brownian motion of defects and dislocations, as well as correlated motion of defects and dislocations mediated by elastic interactions.

Highly glissile prismatic dislocation loops are produced by irradiation [2,3] together with sessile cavities, as evidenced by *in situ* transmission electron microscopy (TEM) observations [4,5]. The correlated motion of dislocation loops, often observed experimentally, is an elementary process leading to the formation of rafts of defects and their eventual coalescence [6–9]. In other words, the spatial ordering of dislocation loops stems from their elastic interaction, whereas the loop motion itself is a thermally activated process, fundamentally the same as stochastic Brownian motion of individual defects [9–14]. The subject of this paper is the simulation of stochastic glide motion of prismatic $a/2\langle 111\rangle$ dislocation loops in body-centered cubic (bcc) iron, with a particular emphasis on the analysis of elementary reactions between the loops, treated as dislocation line objects, and modeled using discrete dislocation dynamics.

Molecular dynamics and lattice type simulations performed over the past two decades investigated the stochastic diffusion of prismatic loops over a range of sizes and temperatures [10–12,15–18], elementary loop and dislocation reactions [1,9], as well as energies of binding of loops to other defects [19]. However, a direct atomistic simulation of an ensemble of interacting dislocation loops still remains a challenge because of the constraint imposed by the simulation cell size accessible to a molecular dynamics simulation, and the relatively short timescale of such a simulation. While the more recent atomistic approaches involving the use of kinetic Monte Carlo [20–23] have reached the experimentally relevant timescale when exploring the relaxation of radiation cascade damage in thin films, the identification of pathways of migration and reaction between interacting dislocation loops containing more than a few dozen interstitials remains a largely unexplored problem.

Discrete dislocation dynamics (DDD) provides a compelling alternative approach to modeling complex dislocation microstructures, offering highly efficient computation of long-range elastic interactions. Furthermore, dislocation dynamics enables the treatment of dislocation reactions, simultaneously simulating internal and collective dislocation loop dynamics, and enabling the investigation of complex networks and junctions within the same methodological framework. We note that bringing dislocation core properties on par with atomistic

*yang.li@cea.fr
†max.boleininger@ukaea.uk
‡christian.robertson@cea.fr
§laurent.dupuy@cea.fr
‖sergei.dudarev@ukaea.uk

simulations remains a challenge, and there have been recent extensive developments addressing this issue [24–32].

The objective of this work is to include thermal stochastic forces in DDD through the Langevin stochastic formalism, to enable modeling the Brownian motion and diffusion of dislocations. The stochastic dislocation dynamics [33,34] approach is formulated and applied to the treatment of diffusion of loops and elementary reactions between interacting loops as an essential step towards modeling thermal evolution of complex dislocation ensembles.

Langevin dynamics has been applied earlier to the treatment of collective dynamics of dislocation loops on a coarse-grained level, where the loops were treated as pointlike objects interacting through long-range elastic fields described in the elastic dipole tensor approximation [1,9,35,36]. Extending the treatment to the case where loop dynamics involves also the relaxation of their internal degrees of freedom, such as tilting of the loop habit plane, we find that this strongly increases the lifetime of configurations where pairs of loops are bound together by their attractive elastic fields. Furthermore, the barriers to entering such bound states are strongly reduced, explaining why dislocation loop rafts are able to form so easily in many materials, as confirmed by *in situ* TEM observations [1,9,37].

The paper is organized as follows. In Sec. II we derive an expression for thermal stochastic forces acting on a dislocation line. In Sec. III the diffusion coefficient of a single prismatic loop is evaluated and examined as a function of temperature, and the DDD analysis is benchmarked against molecular dynamics simulations. We also discuss the fluctuation-dissipation theorem, relating the amplitude of stochastic thermal forces to the magnitude of dissipative drag experienced by a dislocation moving through a crystal. Next, the concept of the loop-loop interaction potential energy surface is introduced, and the elementary loop-loop reactions are simulated, with particular attention devoted to the investigation of internal degrees of freedom of the loops. Finally, in Sec. IV we evaluate the lifetime of an elastically confined loop-loop configuration, which is a functional of the loop-loop interaction potential energy surface.

II. SIMULATION METHOD

A. Stochastic force in dislocation dynamics

All the simulations described in this paper were performed using the 3D nodal dislocation dynamics code NUMODIS [38]. In NUMODIS, continuous dislocation lines are discretized into a series of nodes linked by straight dislocation segments. The internal elastic stress is then computed according to the nonsingular isotropic elasticity theory [39]. The Langevin equation of motion for every point on a dislocation segment is based on the dynamic equation of motion, taken here in the overdamped limit [40]:

$$\mathrm{B}\cdot\boldsymbol{v} = \boldsymbol{f}^{\mathrm{tot}} + \boldsymbol{f}^{s}, \tag{1}$$

where $\boldsymbol{v}$ is the velocity of the dislocation line, B is the viscous drag tensor per dislocation line unit length depending on the slip system and temperature, and $\boldsymbol{f}^{s}$ is the stochastic force per unit length. The presence of a stochastic force introduces time-dependent thermal fluctuations in the dynamics of the dislocation network, resulting from the coupling between mobile dislocations and the heat bath.

The total configurational force per unit length $\boldsymbol{f}^{\mathrm{tot}}$ exerted on a dislocation segment equals

$$\boldsymbol{f}^{\mathrm{tot}} = \boldsymbol{f}^{\mathrm{el}} - \nabla E^{\mathrm{core}}. \tag{2}$$

In the absence of external body and image forces, the elastic driving force $\boldsymbol{f}^{\mathrm{el}}$ reduces to the well-known Peach-Koehler (PK) force. The core energy E^{core} is a phenomenological correction describing the effect of nonlinear interactions in the dislocation core region, which is not taken into account in the linear elasticity approximation. The core energy is also required to yield a net positive line tension for small-scale line fluctuations [29,41], which are expected to arise from the action of stochastic force. The core energy per unit length of a dislocation line here is given in the line tension approximation as [42]

$$E^{\mathrm{core}} = \frac{\xi\mu b^2}{4\pi(1-\nu)}(1-\nu\cos^2\psi(l)), \tag{3}$$

where ξ is the core strength parameter, ψ is the angle between the dislocation tangent and the Burgers vector, and l is the coordinate of a point on a dislocation line.

Consider the intrinsic mobility of an individual prismatic loop with perimeter L in an infinite medium in the absence of external forces. Without loss of generality, assume that the Burgers vector of the loop is collinear with the z direction of the Cartesian system of coordinates. In the absence of climb forces, the motion for a dislocation line is one dimensional:

$$B\frac{\partial z(l,t)}{\partial t} = f_z^{\mathrm{tot}}(l,t) + f^{s}(l,t), \tag{4}$$

where B is the viscous drag coefficient for the given slip system and the stochastic force f^{s} is assumed to be uncorrelated in time and space:

$$\begin{aligned}\langle f^{s}(l,t)\rangle &= 0,\\ \langle f^{s}(l,t)f^{s}(l',t')\rangle &= \sigma_s^2\delta(l-l')\delta(t-t'),\end{aligned} \tag{5}$$

where σ_s sets the scale of the stochastic force, and $\delta(x)$ is the Dirac delta-function

$$\delta(x) = 0, \quad \forall x \neq 0, \qquad \int_{-\infty}^{\infty} dx\,\delta(x) = 1. \tag{6}$$

To find the amplitude of stochastic force, the effective diffusion coefficient for the center-of-position (COP) of the prismatic loop is matched to a 1D Einstein diffusion law [18]. The projection of the COP on the Burgers vector direction is given by $z_{\mathrm{COP}} = L^{-1}\int_0^L dl\; z(l,t)$. After a rearrangement, Eq. (4) becomes

$$\frac{\partial z_{\mathrm{COP}}}{\partial t} = \frac{1}{BL}\int_0^L dl\; f^{s}(l,t). \tag{7}$$

The effect of internal elastic force on the COP vanishes due to the boundary condition $z(l+L,t) = z(l,t)$. Assuming that the initial position of the loop center is $z_{\mathrm{COP}}(0) = 0$, the solution to Eq. (7) at time τ is

$$z_{\mathrm{COP}}(\tau) = \frac{1}{BL}\int_0^L dl\int_0^\tau dt\; f^{s}(l,t). \tag{8}$$

Since the stochastic force $f^s(l,t)$ is defined in terms of its correlation function, the mean square displacement of the COP can be expressed as

$$\langle z^2_{\mathrm{COP}}(\tau)\rangle = \left(\frac{1}{BL}\right)^2 \int_0^L dl \int_0^L dl' \times \int_0^\tau dt \int_0^\tau dt' \langle f^s(l,t) f^s(l',t')\rangle. \quad (9)$$

Substituting Eq. (5) into Eq. (9) yields

$$\langle z^2_{\mathrm{COP}}(\tau)\rangle = \left(\frac{\sigma_s}{BL}\right)^2 \int_0^L dl \int_0^L dl' \times \int_0^\tau dt \int_0^\tau dt' \delta(l-l')\delta(t-t'). \quad (10)$$

Evaluating the above integral, we arrive at

$$\langle z^2_{\mathrm{COP}}(\tau)\rangle = \left(\frac{\sigma_s}{BL}\right)^2 L\tau \equiv 2D_{\mathrm{COP}}\tau. \quad (11)$$

This equation is a mere corollary of the 1D Einstein diffusion law, where D_{COP} is the corresponding diffusion coefficient of the center-of-position [43]. Substituting the fluctuation-dissipation theorem [44]

$$D_{\mathrm{COP}} = \frac{k_{\mathrm{B}}T}{BL} \quad (12)$$

into Eq. (11), which holds under the assumption that the dislocation loop is in thermodynamic equilibrium with the thermostat, we find the amplitude of the stochastic force

$$\sigma_s = \sqrt{2k_{\mathrm{B}}TB}, \quad (13)$$

where k_{B} is the Boltzmann constant and T is absolute temperature.

As NUMODIS is a nodal dislocation dynamics code, the total force per unit length is converted into an effective nodal force by integrating over the neighboring segments [40]. The same rule is applied to convert the stochastic force per unit length into a stochastic force acting on a node. However, care must be taken when rescaling the force, as the randomly applied force must remain consistent with the choice of the segment length and the integration time step. For a straight segment of length Δl indexed by n, the scaled stochastic force per unit length is found using the stochastic average:

$$f^s_n(t) = \frac{1}{\Delta l}\int_{l_n-\Delta l/2}^{l_n+\Delta l/2} dl\; f^s(l,t). \quad (14)$$

Using Eq. (5), for the δ-correlated force generated by thermal fluctuations, the nodal correlation function acquires the form

$$\langle f^s_n(t) f^s_{n'}(t')\rangle = \frac{\sigma_s^2}{(\Delta l)^2}\int_{l_n-\Delta l/2}^{l_n+\Delta l/2} dl \int_{l_{n'}-\Delta l/2}^{l_{n'}+\Delta l/2} dl' \times \delta(l-l')\delta(t-t') = \frac{\sigma_s^2}{\Delta l}\delta_{n,n'}\delta(t-t'). \quad (15)$$

Similarly, assuming an integration time step of Δt, the scaled stochastic force per unit length can be finally expressed as

$$f^s_n = \sqrt{\frac{2k_{\mathrm{B}}TB}{\Delta l\,\Delta t}}N(0,1), \quad (16)$$

where $N(0,1)$ is a random number sampled from the standard normal distribution, and the direction of the force is collinear with the Burgers vector of the dislocation loop.

B. Simulation setup, parameters, and statistics

All the dislocation dynamics (DD) simulations were performed assuming an infinite elastic medium. The coordinate system is chosen as orthogonal with axes parallel to $x = [\bar{1}\bar{1}2]$, $y = [1\bar{1}0]$, and $z = [111]$ directions. Initially, a hexagonal prismatic $\langle 111\rangle$ dislocation loop is positioned at the origin. The loop radius is chosen as $\rho = 4.5$ nm, corresponding to the loop perimeter of $L = 27$ nm. The hexagonal loop shape was chosen out of convenience as this has an almost negligible effect on its dynamics. A circular loop of equivalent size would have the radius of 4.09 nm, representing an inclusion containing the same amount of matter.

The three parameters included in the stochastic force (16) require further clarification.

The viscous drag coefficient B characterizes the drag force acting on a dislocation line. In bcc metals it is generally assumed that $B(T) = B_0 + B_1T$, where B_0 and B_1 are independent of temperature [24,45,46]. MD simulations of glissile prismatic loops and self-interstitial clusters in bcc metals show that $B(T) = B_0$ and is independent of T over a wide temperature range. Given that the simulations performed in this study address prismatic dislocation loops of very small size, it is appropriate to treat B as a temperature-independent constant. The numerical value of B used in this work has been evaluated from the atomistic study by Derlet *et al.* [18] using the fluctuation-dissipation relation (12). The resulting value of the drag coefficient $B = 0.08$ MPa ns describes the effective mobility of edge dislocations at temperatures above $T = 200$ K, but underestimates the magnitude of drag at lower temperatures, as shown in Fig. 1. At low temperatures, the Peierls barrier [47,48] and quantum effects [49,50] play an important part, affecting dislocation mobility, but are not considered in this study. The chosen value of $B = 0.08$ MPa ns agrees well with previous parametrizations derived from the analysis of dislocation-defect interactions in bcc iron [51,52].

Since the simulations were performed by splitting dislocation loops into straight segments, and involved solving the equations of motion by means of a finite difference time integration algorithm, it would be appropriate to assess the effect of discretization length Δl and time step Δt on the computed diffusion coefficient. Thermal diffusion of a single prismatic loop at 300 K was simulated using three discretization lengths, $\Delta l = 5$, 10, and 15 Å, and three time steps, $\Delta t = 0.2$, 0.5, and 1.0 fs. Simulations were run over the interval of 6 ns, with the loop configuration data recorded every 0.6 ps. Loop diffusion coefficients were computed using the drift diffusion correction method [18], in which the diffusion trajectory was split into multiple uncorrelated sub-trajectories. The velocity autocorrelation function $\langle v_{\mathrm{COP}}(t)v_{\mathrm{COP}}(t+\tau)\rangle$ yields the correlation time of $\tau \approx 2$ ps, in broad agreement with atomistic estimates [13,29]. The velocity correlation time is longer

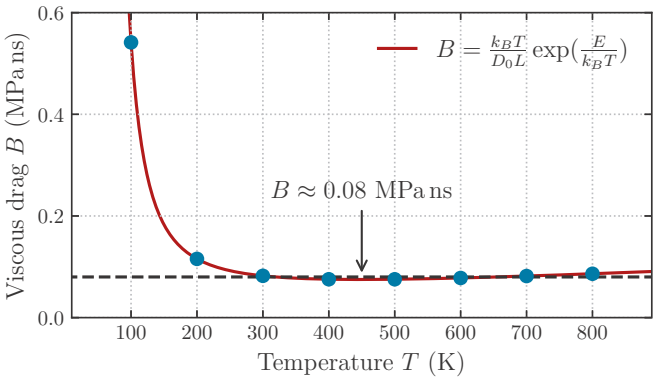

FIG. 1. Viscous drag coefficient B for a prismatic dislocation loop in bcc iron extracted from molecular dynamics simulations [18] (dots). The viscosity is well described by a non-Arrhenius relation (line), see Derlet *et al.* [18] for the choice of parameters in the functional expression. The dashed line corresponds to the constant value of $B = 0.08$ MPa ns used here, which is valid for temperatures above 200 K.

than the stochastic force correlation time [45] derived from atomistic simulations, and represents the low limit for the time length of a subtrajectory, which here was chosen as 6 ps. The diffusion coefficient is then found by ensemble averaging over the subtrajectories, with the uncertainty characterized by the standard error of the mean.

Figure 2 shows a selection of simulated COP trajectories, which are similar in terms of their statistical properties. The values of diffusion coefficient derived from these trajectories remain within their respective error bounds, independent of the selected values of Δl and Δt, in agreement with the theoretical analysis by Derlet *et al.* [18].

Following Scattergood and Bacon [53], the elastic moduli μ and ν are chosen by matching the isotropic and anisotropic elasticity energies of infinite $a/2\langle 111\rangle\{110\}$ edge and screw dislocations. Earlier comprehensive studies [54–56] confirm that this method leads to highly accurate predictions of dislocation loop shapes and stress fields. In this work, the anisotropic moduli used as input were chosen following

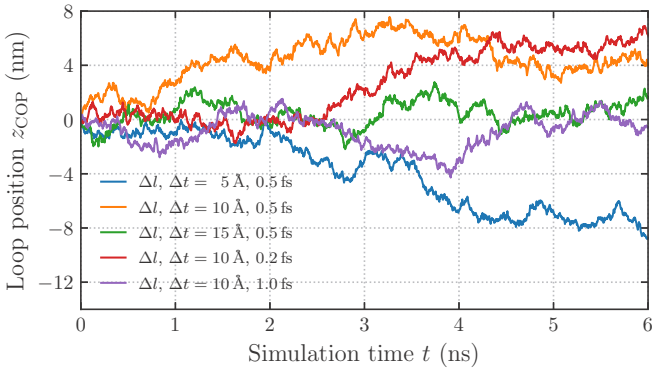

FIG. 2. Random walk trajectories of a prismatic loop with radius $\rho = 4.5$ nm undergoing Brownian motion at 300 K simulated using the same viscous drag coefficient, and several different discretization lengths Δl and time steps Δt. The diffusion behavior of the loop is independent of the choice of discretization parameters.

TABLE I. Simulation parameters for pure bcc iron [51,58].

Parameter	Symbol	Value
Burgers vector	b	2.47 Å
Shear modulus	μ	63 GPa
Poisson's ratio	ν	0.43
Drag coefficient	B	0.08 MPa ns
Dislocation core radius	R_c	1.4 Å
Core strength parameter	ξ	0.257
Time step	Δt	0.5 fs
Discretization length	Δl	10 Å

Ackland *et al.* [57] as $C_{11} = 225$ GPa, $C_{12} = 124$ GPa, and $C_{44} = 101$ GPa, leading to the corresponding isotropic moduli of $\mu = 63$ GPa and $\nu = 0.43$.

The dislocation core radius R_c, which here has the same meaning as the delocalization parameter of the nonsingular elasticity theory [39], and the core strength parameter ξ were evaluated in earlier studies [51,58] from atomistic simulations.

Isotropic elasticity theory represents an effective approximation for bcc iron, which is an elastically anisotropic material. The numerical results presented in this work should therefore be interpreted qualitatively. This is a foregone conclusion if we acknowledge the fact that the commonly accepted models for the dislocation core energy do not capture the complex anisotropic configurational energy landscape found in atomistic simulations. The stochastic forces formalism itself is directly applicable to DDD simulations in elastically anisotropic materials.

All the further simulations presented in Sec. III were carried out using the simulation parameters given in Table I, unless specified otherwise. The integration time step scales approximately as a cube of the dislocation discretization length, see Appendix A. We have opted to use a fine time step and small discretization length, as computational efficiency and performance was not a concern in the simulations presented here.

III. RESULTS

A. Stochastic dynamics of an individual dislocation loop

Using stochastic dislocation dynamics, we performed a series of simulations, investigating the dynamics of a single prismatic loop at temperatures ranging from 100 to 800 K, with temperature increments of 100 K. No external stress was applied.

Consider first the internal degrees of freedom of the prismatic loop. It is readily seen from simulations that the initially purely prismatic [111] loop with its Burgers vector normal to its habit plane, within a few picosecond adopts a tilted configuration, see Fig. 3(a). If the shape of the loop is defined by its dislocation countour C, the *vector* area of the loop is given by [36,59]

$$\boldsymbol{A} = \frac{1}{2}\oint_C \boldsymbol{r} \times d\boldsymbol{l}, \tag{17}$$

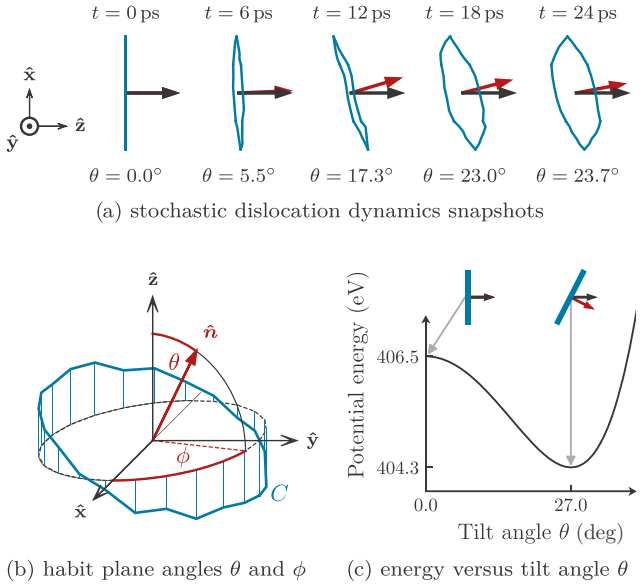

FIG. 3. (a) Snapshots from a stochastic dislocation dynamics simulation of a hexagonal initially pure prismatic loop of 4.5 nm radius at 100 K show that the loop habit plane becomes tilted within a few picoseconds. (b) The tilt angle θ is defined as the angle between the normal vector (red arrow) and the Burgers vector (black arrow). (c) The prismatic loop adopts a tilted configuration on the glide cylinder to minimize its potential energy.

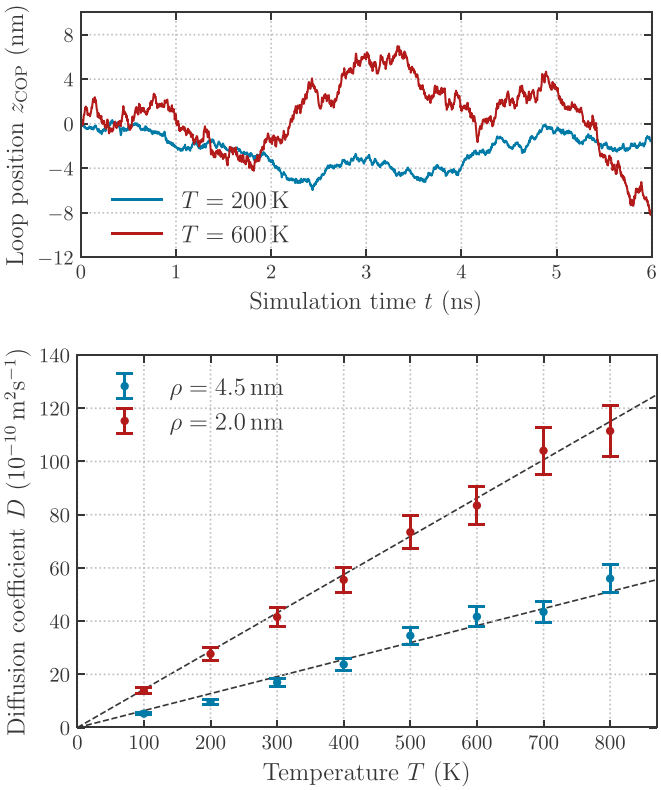

FIG. 4. Top: Random walk trajectories of a hexagonal prismatic loop of radius $\rho = 4.5$ nm simulated for 200 and 600 K. Bottom: Plots of diffusion coefficients as a function of temperature for different loop sizes ρ. Dashed lines are analytical predictions derived from the fluctuation-dissipation theorem $D_{COP} = k_B T/(BL)$.

and the effective loop normal unit vector is

$$\hat{\boldsymbol{n}} = \frac{1}{2||\boldsymbol{A}||} \oint_C \boldsymbol{r} \times d\boldsymbol{l}. \tag{18}$$

The angle between the Burgers vector and the effective loop normal shall be referred to as the tilt angle θ, with the azimuthal angle ϕ defined in full analogy with the spherical system of coordinates, see Fig. 3(b) for illustration. Following this definition and depending on the nature of the loop (vacancy or interstitial), the loop is pure prismatic if $\hat{\boldsymbol{n}} \cdot \hat{\boldsymbol{b}} = \pm 1$ corresponding to $\theta = 0$ or 180°. We note that the elastic relaxation volume of a loop is given by the scalar product of the Burgers vector and the loop vector area $\Omega_{rel} = \boldsymbol{b} \cdot \boldsymbol{A}$ [36].

The elastic potential energy of a prismatic loop is minimized for configurations tilted away from the perfect prismatic loop orientation, with the resulting tilt angle θ determined by the competition between the elastic self-energy associated with interaction between dislocation segments and the core energy proportional to the length of the perimeter of the loop, see Fig. 3(c). The potential energy is invariant with respect to rotations around the Burgers vector, allowing the loop to rotate freely with respect to ϕ in a DD simulation.

The mean value of the tilting angle $\langle\theta\rangle$ decreases at higher temperatures, reflecting the anharmonicity of the potential self-energy of the loop. Indeed, it takes comparatively less energy for the loop normal to tilt towards the Burgers vector than away from it, hence on average smaller values of θ are favored at higher temperature.

In addition to the tilting degrees of freedom, the loop shape also develops transient fluctuations on a smaller scale. However, any part of the loop is constrained to remain on the glide cylinder, as the relaxation volume of the loop $\Omega_{rel} = \boldsymbol{b} \cdot \boldsymbol{A}$ is conserved throughout the simulation.

Consider next the diffusion behavior of the entire loop. The prismatic loop trajectories exhibit a characteristic pattern of Brownian motion, with higher temperature inducing a more pronounced loop displacement per unit time. The single loop COP trajectories for 200 and 600 K, and the diffusion coefficients calculated with the drift diffusion correction [18], are given in Fig. 4. Globally, the temperature dependence of the diffusion coefficient is found to be consistent with the fluctuation-dissipation theorem, regardless of the loop radius ρ.

Moreover, for $\rho = 4.5$ nm and $T < 400$ K the diffusion coefficients derived from simulations are consistently lower than expected from the linear interpolation from higher temperature (dashed line) because the tilting of the loop results in the elongation of its perimeter, see Fig. 3(b). According to the fluctuation-dissipation theorem, $D_{COP} \propto 1/L$, and therefore the reorientation of the habit plane gives rise to a lower value of the diffusion coefficient. This effect is found to become less pronounced at higher temperature as the mean tilt angle $\langle\theta\rangle$ decreases with temperature.

The stochastic DD simulations performed in this work describe thermally induced Brownian motion of prismatic loops, which for $T > 200$ K is consistent with molecular dynamics. The simulations further reveal that the prismatic loop habit plane becomes tilted with respect to the Burgers vector, while

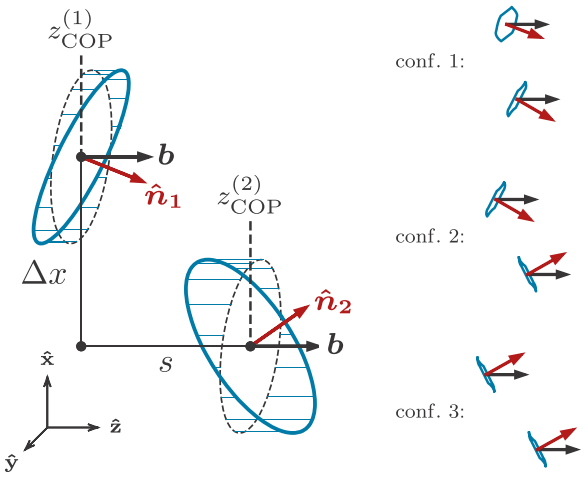

(a) Two interacting loops (b) metastable configurations of loops

FIG. 5. (a) Two prismatic loops defined using the coordinate system introduced in Sec. III B, with identical Burgers vectors $\boldsymbol{b}$ parallel to z direction. Loop configuration (line) is free to deviate from the pure prismatic form (dashed) on the glide cylinder, as indicated by the loop normal vectors $\hat{\boldsymbol{n}}$. (b) A selection of representative metastable configurations of interacting loops extracted from dislocation dynamics simulations, also showing the loop normal and Burgers vectors. Configurations are ordered from top to bottom in the order of increasing stability, and hence in the order of descending total potential energy. Configuration 3 is the most stable configuration.

remaining highly mobile with respect to rotations around the Burgers vector.

The tilting behavior of prismatic loops in atomistic simulations is possibly dominated by singular orientation effects in the core energy [60]. Considering that the core energy scales linearly with the loop radius $\propto \rho$, whereas the elastic self-energy varies superlinearly as $\propto \rho \log \rho$ [61], one would expect the core energy to become less significant for larger loops. However, the singular nature of the core energy in combination with atomic discreteness would break the cylindrical symmetry of the system, subsequently introducing energy barriers in relation to its rotation around the Burgers vector.

B. Diffusion of interacting dislocation loops

The question about thermal evolution of interacting dislocation loops has recently attracted attention in the context of dipole tensor formalism as an efficient approximation for the long range elastic interaction between the loops [35,62]. Here we show that the internal degrees of freedom of loops, not explicitly treated by the dipole tensor formalism, have a profound effect on the stochastic dynamics of loops, particularly where the loops form bound configurations confined by attractive elastic interactions.

Consider a pair of prismatic loops with unit Burgers vectors $\hat{\boldsymbol{b}}_1 = \hat{\boldsymbol{b}}_2 = \hat{z}$. The loop centers are separated by distance s in the glide direction and by Δx in the direction perpendicular to the Burgers vector direction, see Fig. 5(a). In the absence of climb force, either loop can move or distort only in the glide direction.

While the stochastic simulations involve an explicit treatment of internal degrees of freedom of the loops, it is also instructive to consider the static properties of a simplified system of two loops. Following the discussion in Sec. III A, the internal degrees of freedom of the simplified system are reduced to the tilting modes only, thus keeping the loops otherwise flat and of ellipsoidal shape.

For a single loop the potential energy is invariant with respect to rotations around its Burgers vector. For a pair of loops the invariance is lifted by their elastic interaction: for a loop-pair separation constrained at s, the system has multiple tilting configurations corresponding to local energy minima, giving rise to a complex potential energy surface (PES) with several branches and crossing points. In full analogy to the Born-Oppenheimer approximation [63], the internal degrees of freedom of loops evolve significantly faster (on the timescale of ∼ps) than the loop-pair separation (varying on the ∼ns timescale), and thus the notion of PES describes the system of interacting loops in the adiabatic approximation. Each PES branch represents a metastable tilting state for a given reaction coordinate s. Transitions between PES branches occur by the rotation of loop habit planes, which are therefore separated by energy barriers.

The energy of interaction between pairs of prismatic loops is computed in the order of ascending accuracy: in the dipole tensor approximation for a pair of pure prismatic loops, as exact elastic interaction between a pair of pure prismatic loops, and as exact elastic interaction between prismatic loops with internal degrees of freedom relaxed to metastable configurations. Note that in the dipole tensor approximation the expression for the loop-loop interaction in the pure prismatic case reduces to the Foreman-Eshelby expression [1,2,64]. The treatment of internal relaxation is explained in detail in Appendix B. The energy of interaction between the loops is defined as the energy difference between the total energy of two loops minus the energy of isolated loops with the same orientation of the Burgers vector:

$$W^{\mathrm{int}}(s) = W^{\mathrm{tot}}(s) - \lim_{s\to\infty} W^{\mathrm{tot}}(s). \tag{19}$$

Energies of elastic interaction are compared in Fig. 6 for the various loop separations Δx using an example of two round loops with radii $\rho = 4.09\,\mathrm{nm}$. Note that the choice of radii is consistent with loops being hexagonal and having the same area, as discussed in Sec. II B.

The exact interaction energy trend for pure prismatic pairs of loops broadly follows the PES trend, but does not reflect the full complexity of interaction between internally relaxed loops. The dipole approximation is consistent with the exact treatment, but only for loop separations several times larger than the sum of loop radii. The dipole tensor formalism becomes inaccurate for smaller separations, resulting in a qualitatively incorrect predicted interaction behavior, see the top two panels in Fig. 6.

A major effect of internal relaxation is found when we follow how the loops approach an elastically confined bound state from infinite separation. This reaction is fundamental to the formation of dislocation loop rafts. From Fig. 6 it is

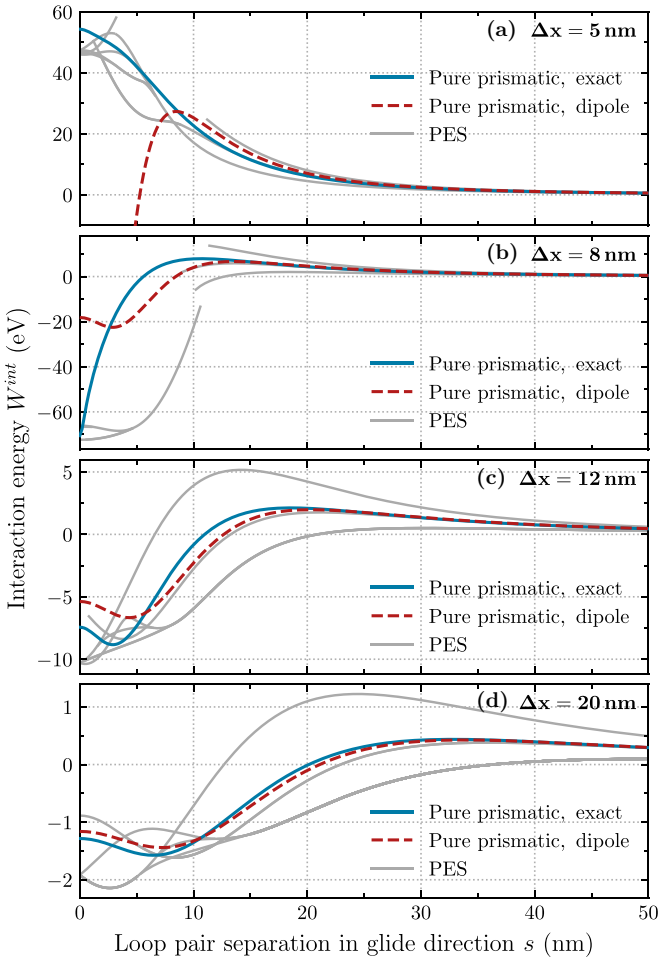

FIG. 6. Comparison of energies of elastic interaction of two pure prismatic dislocation loops of radius $\rho = 4.09$ nm, obtained by exact integration (solid, blue) and computed in the dipole tensor approximation using the Foreman-Eshelby equation [1,2,64] (dashed, red). Allowing the loops to tilt, and thus to acquire a mixed character, reveals a complex potential energy surface (solid, gray). Plots (a) to (d) represent loop pairs with increasing separation Δx perpendicular to the glide cylinders.

evident that loop interaction energy at large separations is positive. Therefore an energy barrier first has to be overcome before the loops can enter a bound state. This barrier is here given by the maximum value of the chosen potential energy branch. In the pure prismatic loop picture the barrier is substantial, ranging from 8, 2, and 0.4 eV for separations Δx of 8, 12, and 20 nm, respectively. In contrast, the lowest PES branches have dramatically reduced barriers to trapping of 2, 0.5, and 0.1 eV, respectively, and as such may eventually be overcome by diffusion. In our earlier work based on a pure prismatic loop picture, where elastic interaction between the loops was described by the Foreman-Eshelby equation [2,64], the trapping barrier had to be artificially lowered to facilitate elastic confinement of loops, as otherwise no formation of loop rafts would occur [1].

We also note that in the limit of large separation s, only three PES branches form. The corresponding fundamental configurations of pairs of loops are shown in Fig. 5(b), and their energy ordering is consistent with the separations Δx studied here.

This comparison demonstrates that the energy of interaction between prismatic loops is strongly affected by the internal degrees of freedom of the loops. Consequently, the competition between the elastic energy and the core energy plays a pivotal role in determining the landscape of binding energies of loops. This subtlety is neglected in any physical approximation where the dislocation loops are treated as being purely prismatic, or where they are treated as pointlike objects defined only by their position in real space and involving no consideration of their internal degrees of freedom.

In what follows, we carry out stochastic dislocation dynamics simulations of interacting pairs of loops. The simulations start from large initial separations Δx and s at 200 K in an attempt to emulate various elementary interactions observed in experiment, see Sec. I, namely coalescence, repulsion, and mutual elastic confinement of interacting loops.

Case A: Coalescence of dislocation loops

The coalescence of dislocation loops was observed using TEM and was found to involve loops of comparable size [8], with diameters larger than 4 nm. To match experimental observations, two pure prismatic hexagonal ⟨111⟩ loops with $\rho = 4.5$ nm are introduced in a simulation cell with separations of $\Delta x = 8$ nm and $s = 5$ nm, giving rise to a mutually attractive elastic force, see Fig 6. Note that the glide cylinders of the loops overlap slightly. Sequential snapshots taken during simulations are shown in Fig. 7(a). The loops coalesce into a larger prismatic loop, with small debris released and ejected by a strong repulsive elastic force.

The corresponding time evolution of the diffusion coefficient of the resulting large loop is shown in Fig. 7(b). We observe that the diffusion coefficient becomes constant over the interval of a few nanoseconds and converges to a notably smaller value than the diffusion coefficient of a single loop with $\rho = 4.5$ nm. Using the $D_{\mathrm{COP}} \propto 1/L$ scaling relation, the equivalent loop size of the loop produced by the coalescence of a pair of loops equals $\rho_{\mathrm{eq}} \approx 7$ nm. This is consistent with an estimate of the equivalent loop size obtained by removing a quarter of each loop's circumference, leading to $\rho_{\mathrm{eq}} \approx 3/2\rho$. While the relaxation volume of the loops is a conserved quantity, the length of the loop circumference is not; this example demonstrates clearly that the effective diffusivity of an ensemble of prismatic loops may reduce over time as a result of coalescence of loops.

Case B: Repulsion between the loops

An example of repulsive interaction between diffusing dislocation loops is obtained by placing the loops with separations of $\Delta x = 5$ nm and $s = 7$ nm, using the different initial configurations shown in Fig. 5(b). Note that configuration 1 was placed at a separation of $s = 12$ nm, as its corresponding PES branch vanishes at closer separations. Figure 8 shows the evolution of the corresponding interaction energies during the simulation performed without stochastic forces ($T = 0$ K) and with stochastic forces ($T = 200$ K) included, in comparison with the theoretical prediction derived from examining the corresponding potential energy surface.

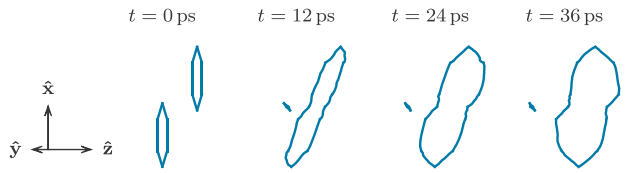

(a) snapshots illustrating the dynamics of coalescence of loops

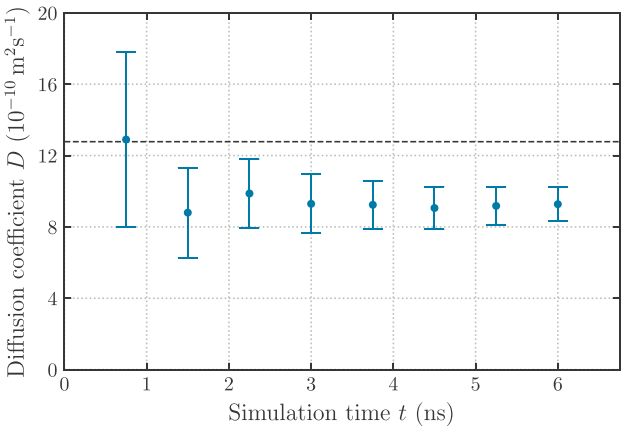

(b) diffusion coefficient as a function of time

FIG. 7. (a) Shapshots taken from stochastic dislocation dynamics simulations of a loop coalescence reaction, for the initial loop-pair separations of $\Delta x = 8\,\text{nm}$ and $s = 5\,\text{nm}$, viewed at an angle from the $-\hat{\mathbf{y}}$ direction. Note the occurrence of ejection of debris during loop coalescence. (b) Plot of the effective diffusion coefficient as a function of time. The dotted line is a reference value computed for a single loop with size $\rho = 4.5\,\text{nm}$.

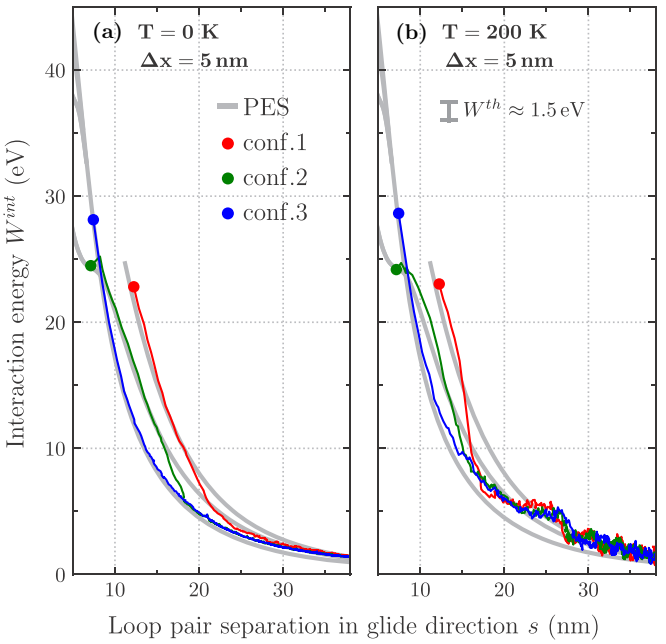

FIG. 8. Dislocation dynamics simulation of two prismatic loops in a repulsive arrangement without (a) and with stochastic forces at $T = 200\,\text{K}$ (b) included. The initial loop configurations (conf.) are taken from Fig. 5. Trajectories in (b) are shifted down by an estimated amount of additional thermal energy supplied by the thermostat W^{th} for better comparison. In the absence of stochastic forces the system of two loops moves along the PES branches, see conf. 1 and conf. 3 in (a). On the other hand, the trajectories of the heated system eventually become indistinguishable, oscillating between various tilting configurations.

As expected for repulsive configurations, we find that the distance between the loops gradually increases over the interval of time spanned by the simulation. Inspection of the loop-pair configuration shows that the cold ($T = 0\,\text{K}$) systems retain their initial orientation of the habit plane, which is consistent with the energy trajectories propagating along the distinct PES branches. On the other hand, the trajectories of the heated system ($T = 200\,\text{K}$) soon start overlapping, starting from $s \approx 20\,\text{nm}$, eventually becoming indistinguishable. The stochastic force supplies additional thermal energy to the loops, which is evidently sufficient to overcome the energy barrier between the different PES branches, enabling the loops to rotate and thus oscillate between various tilting configurations.

Case C: Elastic confinement of loops

Prismatic loops may exhibit strong elastic attraction and form an elastically confined configuration as seen in Fig. 6. Depending on loop size and loop separation, the binding energy can vary from meVs to eVs, potentially surpassing the binding energy of dislocations to substitutional defects. Therefore it can be reasoned that elastic confinement of loops represents the key step leading to the stabilization of experimentally observed rafts of dislocation loops.

We adopt the initial setup corresponding to $\Delta x = 12\,\text{nm}$ and $s = 12\,\text{nm}$, for which the pair of loops exhibit mutual attraction. As in the repulsive case investigated above, the simulations were run for three initial loop configurations shown in Fig. 5(b), corresponding to distinct branches of the potential energy surface. The evolution of the energy of interaction between the two loops as a function of their separation in comparison with the idealized PES is shown in Fig. 9.

In the absence of stochastic forces, the two-loop system is hindered from reaching the lowest energy state because it is unable to overcome the energy barrier associated with the rotation of the loop habit planes. In contrast, the addition of stochastic forces supplies the loops with additional energy, enabling the system to explore the potential energy landscape more freely to the point where it even oscillates around the global energy minimum. As in the loop repulsion case investigated above, the interaction energy derived using simulations involving elevated temperature is found to be shifted upwards by about 1.5 eV compared to the PES, as the Langevin thermostat adds additional energy to the system.

The COP trajectories of the two loops corresponding to conf. 1 state are shown in Fig. 10. After a brief initial relaxation time, the loops become mutually trapped in their relative frame by attractive elastic interaction, with their COP trajectories becoming strongly spatially correlated. The loop separation distance in the elastically confined state fluctuates around the global potential energy minimum as a result of the effect of stochastic force, in agreement with experimental observations and simulations reported in Figs. 3–5 of Ref. [1]. Interestingly, the simulated trajectories suggest that the two bound loops oscillate on a ∼0.5 ns timescale, thus evolving significantly slower than the tilt angle of the isolated loop, see Fig. 3.

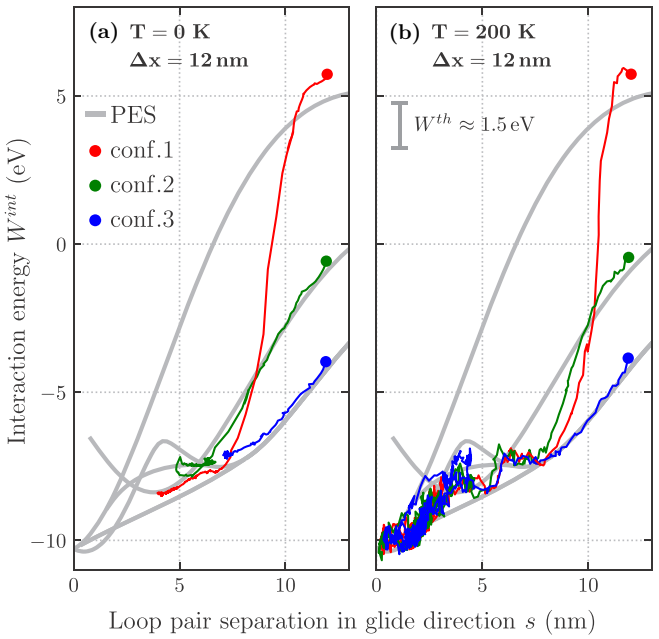

FIG. 9. Dislocation dynamics simulation of a pair of prismatic loops in an attractive arrangement without (a) and with stochastic forces at $T = 200$ K (b) included. The initial configurations (conf.) of loops are taken from Fig. 5. Trajectories in (b) are shifted down by an estimated amount of additional thermal energy supplied by the thermostat W^{th} for better comparison. In the absence of stochastic forces, the loop pair is stuck in metastable configurations. In contrast, the heated system escapes from the metastable state, instead fluctuating around the global minimum.

IV. THE LIFETIME OF ELASTICALLY CONFINED LOOP CONFIGURATIONS

In Sec. III B above, we have explored the three types of fundamental reactions between prismatic dislocation loops. These reactions, namely loop coalescence, repulsion, and mutual elastic trapping or confinement, have all been modeled using stochastic dislocation dynamics at 200 K. The simulations enable comparison with models developed earlier for simulating the thermal evolution of multiple loops, which involve the dipole approximation [9] and treat the loops as point objects, assuming that they remain purely prismatic

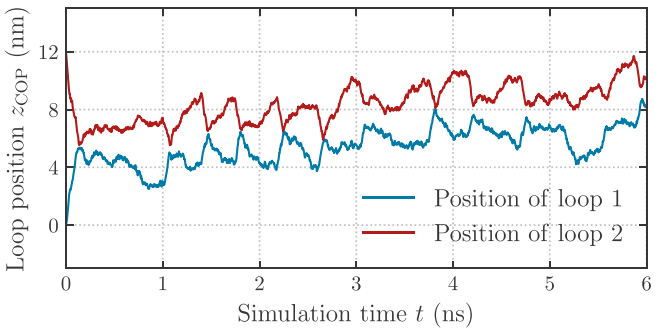

FIG. 10. z coordinates of centers of elastically confined loops plotted versus simulation time. The initial position of the loops corresponds to conf. 1.

over the duration of the simulation. In this paper we show that the internal degrees of freedom significantly influence the nature of interaction between the loops, with potentially significant implications for the lifetime of elastically confined loop configurations. We now analyze this effect quantitatively.

Introducing the probability density $P(s,t)$ of finding the two loops at separation s at time t, the equation of motion for this probability density, see Appendix C, can be expressed as a Fokker-Planck equation [65–67]

$$\frac{\partial P(s,t)}{\partial t} = -\frac{\partial J(s,t)}{\partial s}, \tag{20}$$

where J is the flux of the probability density

$$J(s,t) = -\frac{2}{\beta BL} e^{-\beta V(s)} \frac{\partial}{\partial s}\left(e^{\beta V(s)} P(s,t)\right), \tag{21}$$

where $\beta = 1/(k_{\text{B}}T)$ and $V(s)$ refers to a branch of the potential energy surface. It is sufficient to consider the $s \in [0, +\infty)$ interval of variation of s as the potential energy surface is symmetric. In the following discussion we assume that the potential energy surface includes a confined state that transforms, over an energy barrier, into an unbound state at large separation s. While this assumption is valid for a pair of loops, caution needs to be taken in densely populated microstructures, as the potential energy can be strongly distorted by the elastic field of other defects.

Consider now the pair of loops at an energy minimum at s_{min}. At equilibrium steady state the flux vanishes, $J = 0$, leading to the probability acquiring the form of the Gibbs distribution $P(s) \sim \exp[-\beta V(s)]$. Similarly, the escape process from the energy minimum at s_{min} to a very far separation along the glide direction $s_{\text{far}} \gg s_{\text{min}}$ can be considered to proceed slow enough to preserve the steady state, leading to a constant flux $J = J_0$. The steady-state flux is found by solving Eq. (21) for the derivative and subsequently integrating from s_{min} to s_{far}, namely

$$\left[e^{\beta V(s)} P(s)\right]_{s_{\text{min}}}^{s_{\text{far}}} = -\frac{J_0 \beta BL}{2} \int_{s_{\text{min}}}^{s_{\text{far}}} ds\, e^{-\beta V(s)}. \tag{22}$$

Using $P(s_{\text{min}}) \gg P(s_{\text{far}})$, the escape flux can be found as

$$J_0 \approx \frac{2}{\beta BL} \frac{e^{\beta V(s_{\text{min}})} P(s_{\text{min}})}{\int_{s_{\text{min}}}^{s_{\text{far}}} ds\, e^{\beta V(s)}}. \tag{23}$$

Assuming that the probability density decays rapidly outside the potential well associated with the energy minimum, the probability p of finding the pair of loops in an elastically confined state is derived by integration over the well width $\pm\delta s$, using the method of steepest descent

$$\begin{aligned} p &= \int_{s_{\text{min}}-\delta s}^{s_{\text{min}}+\delta s} ds\, P(s) \\ &= P(s_{\text{min}}) \int_{s_{\text{min}}-\delta s}^{s_{\text{min}}+\delta s} ds\, e^{-\beta[V(s_{\text{min}})-V(s)]} \\ &\approx \frac{P(s_{\text{min}})}{2} \int_{-\infty}^{+\infty} ds\, e^{-\beta V''(s_{\text{min}}) s^2/2} \\ &= \frac{P(s_{\text{min}})}{2} \left(\frac{2\pi}{\beta V''(s_{\text{min}})}\right)^{1/2}, \end{aligned} \tag{24}$$

TABLE II. The lifetime of an elastically confined pair of dislocation loops computed for some selected loop radii ρ and temperatures T assuming the separation between the loops in a plane perpendicular to their glide cylinders of $\Delta x = 12$ nm. Three distinct configurations of pairs of loops are considered.

Conditions	Pure prismatic	Lowest PES	30° fixed tilt
$\rho = 4.5$ nm, $T = 200$ K	$\sim 10^{259}$ yr	$\sim 10^{258}$ yr	$+\infty$
$\rho = 4.5$ nm, $T = 600$ K	$\sim 10^{75}$ yr	$\sim 10^{75}$ yr	$\sim 10^{117}$ yr
$\rho = 2.0$ nm, $T = 200$ K	4 s	18 min	3 yr
$\rho = 2.0$ nm, $T = 300$ K	5 ms	0.3 s	5 min
$\rho = 2.0$ nm, $T = 400$ K	0.2 ms	6 ms	0.5 s
$\rho = 2.0$ nm, $T = 500$ K	0.02 ms	0.5 ms	10 ms
$\rho = 2.0$ nm, $T = 600$ K	0.005 ms	0.1 ms	0.8 ms

where $V''(s_{\min})$ is the second derivative of $V(s)$ evaluated at the stationary point $s_{\min}$. Similarly, the integral term in Eq. (23) peaks at the point $s_{\max}$ corresponding to the maximum barrier height. Applying the same approach as in Eq. (24), the escape rate Γ can be finally expressed as

$$\Gamma \equiv \frac{J_0}{p} = \frac{[V''(s_{\min})|V''(s_{\max})|]^{1/2}}{2\pi BL} e^{-\beta \Delta V}, \qquad (25)$$

where $\Delta V = V(s_{\max}) - V(s_{\min})$ is the energy barrier that the pair of loops has to overcome in order to separate. The inverse of the escape rate equals the lifetime of the confined state of the loops. Under these conditions, a small variation of ΔV can significantly affect the lifetime.

Consider now the choice of the potential branch $V(s)$. We use three different tilting configurations to investigate the effect of internal degrees of freedom on the confinement lifetime. First, the pure prismatic pair of loops is a reference configuration to models involving no internal degrees of freedom. Next, the freely tilting loop pair is represented by the lowest energy curve of the PES. Finally, the tilting of each loop is fixed ad-hoc at an angle of 30° each [unfavorable in energy, see conf. 1 in Fig. 5(b)], in an attempt to mimic the habit plane locking observed in molecular dynamics. The corresponding lifetimes of elastically confined loop configurations are listed in Table II for circular loops with $\rho = 4.09$ nm and $\rho = 1.8$ nm, which are equivalent to hexagonal loops with $\rho = 4.5$ nm and $\rho = 2$ nm. In either case the separation between the two loops in the plane perpendicular to the glide cylinders is chosen as $\Delta x = 12$ nm.

Table II shows that the lifetime of the elastically confined configuration depends strongly on the loop size and temperature. For $\rho = 4.5$ nm the pair of loops is effectively unable to escape from the elastically confined state, as the lifetime is dominated by the escape barrier of $\approx$10 eV. On the other hand, the lifetime of an elastically confined configuration involving smaller loops $\rho = 2$ nm is comparable with experimental timescales even at low temperatures.

The specific form of configuration of interacting dislocation loops is found to have a most significant effect on its lifetime. An approximation where the loops are treated as pure prismatic objects underestimates the escape time in comparison with the case of freely rotating loops by several orders of magnitude. In contrast to that, the pair of loop with the orientation of their habit planes fixed at 30° has a significantly longer lifetime in comparison with a freely rotating pair of loops, and it only breaks apart at relatively high temperatures. This offers a possible explanation for why the experimentally observed rafts of loops remain stable over an appreciable temperature range, while a simple estimate based on the purely prismatic picture of interacting loops predicts much shorter lifetimes [1]. The loop habit plane reorientation not only changes the barrier that the system needs to overcome in order to escape, but most importantly it strongly lowers the curvature of the potential energy barrier, see Fig. 6, hence further increasing the lifetime of an elastically confined configuration by several orders of magnitude.

V. CONCLUSION

The stochastic motion of prismatic dislocation loops diffusing in the glide direction is successfully simulated using dislocation dynamics that also includes the stochastic thermal forces treated using the Langevin equation formalism. The dependence of the diffusion coefficient of a dislocation loop on temperature is consistent with molecular dynamics simulations.

Reactions involving interacting dislocation loops, including loop coalescence, repulsion, and the formation of an elastically confined pairs of loops, are well reproduced using the stochastic dislocation dynamics framework proposed above. The internal degrees of freedom of interacting loops result in the formation of complex potential energy landscape of states with distinctly tilted loop habit planes, separated by potential barriers. The addition of thermal energy through stochastic Langevin forces acting on dislocation lines enables interacting loops to switch between the tilted configurations, allowing the system to explore the entire energy landscape of excited states.

In comparison to the purely prismatic case of interacting loops first explored by Foreman and Eshelby [64], the reorientation of the habit plane of interacting loops is found to strongly affect the rates of reactions resulting in the elastic confinement of loops. For one, the potential barrier for the elastic trapping a loop approaching another loop from a distance is strongly reduced, making it much more likely for loops to form elastically trapped configurations. Second, the lifetime of the elastically confined state increases by several orders of magnitude, bringing the estimated lifetime into broad agreement with experimental observations. The habit plane reorientation effect highlights the pivotal significance of including internal degrees of freedom of loops in the treatment of microstructural evolution, to achieve a physically consistent description of dynamics of complex dislocation microstructures.

ACKNOWLEDGMENTS

M.B. and S.L.D. gratefully acknowledge stimulating discussions with D. R. Mason, P. M. Derlet, and D. Rodney. This work has been carried out within the framework of the EUROfusion Consortium and has received funding from the Euratom research and training programme 2014-2018 and 2019-2020 under Grant Agreements No. 633053 and No. 755039. Also, it has been partially funded by the RCUK Energy Programme (Grant No. EP/P012450/1). The views

and opinions expressed herein do not necessarily reflect those of the European Commission. The complementary support of the Materials Research Program RMATE of the Nuclear Energy Division of the French Atomic Energy Commission (CEA/DEN) is acknowledged as well.

APPENDIX A: RELATION BETWEEN THE INTEGRATION TIME STEP AND SEGMENT LENGTH

Here we give an estimate to the maximum time step that can be used for integrating the coupled stochastic equations of motion describing a fluctuating dislocation. We assume that the stochastic force acting on a dislocation node n is greater than elastic forces, and that the adjacent segments have length Δl:

$$B\dot{z}_n(t) \approx f_n^s = \sqrt{\frac{2k_BTB}{\Delta l\,\Delta t}}N(0,1). \tag{A1}$$

We continue by making a conservative assumption that the nodal positions are updated according to Euler's scheme, and that the randomly generated number $N(0,1)$ is equal to three. For the sake of numerical stability in updating the dislocation network, we assert that the node should not move by more than a fraction $q \leqslant 1$ of the segment length, leading to $\dot{z}_n(t)\Delta t \leqslant q\Delta l$. We then arrive at a cubic relation between time step and segment length:

$$\Delta t \leqslant \frac{q^2(\Delta l)^3 B}{18k_BT}. \tag{A2}$$

Using values of $q = 0.1$, $B = 0.08\,\mathrm{MPa\,ns}$, $T = 300\,\mathrm{K}$, and $\Delta l = 10$ Å, we arrive at a maximum allowed time step $\Delta t = 11\,\mathrm{fs}$. Similarly, for $\Delta l = 30$ Å we find $\Delta t = 290\,\mathrm{fs}$. Hence the stochastic simulations of coarsely resolved dislocation networks can proceed with larger time steps than the matching atomistic simulations.

APPENDIX B: POTENTIAL ENERGY SURFACE OF THE LOOP PAIR

Given a vector $\boldsymbol{z}$ containing all the node positions, we define a set of local energy minima that depend parametrically on the distance between the loops:

$$V_S(s) = \{W^{\mathrm{tot}}(\boldsymbol{z}) \mid \boldsymbol{z} \in \mathcal{Z} \text{ is a local minimum}\}, \tag{B1}$$

where

$$\mathcal{Z} = \left\{\boldsymbol{z} \middle| z_{\mathrm{COP}}^{(2)} - z_{\mathrm{COP}}^{(1)} = s\right\} \tag{B2}$$

refers to the set of nodal positions for which the separation between the loops is s. In other words, the loop separation is held constant, whereas the remaining internal degrees of freedom are varied to find local potential energy minima.

The potential energy surfaces defined by Eqs. (B1) and (B2) are found by the numerical minimization of energy of a simplified system of two loops. The internal degrees of freedom are reduced to tilting modes only, leading to the following parametrization of the dislocation loop:

$$\boldsymbol{r}(\psi) = \begin{pmatrix} \rho\cos\psi \\ \rho\sin\psi \\ u\sin\psi + v\cos\psi \end{pmatrix}, \tag{B3}$$

where $\psi \in [0,\ 2\pi)$ is the parametrization variable, and $u \in \mathbb{R}$ and $v \in \mathbb{R}$ are tilting amplitudes. The normal vector of the parametrization is independent of ψ and is free to point in any direction, while the loop relaxation volume is constant as $\Omega_{\mathrm{rel}} = \boldsymbol{b}\cdot\boldsymbol{A} = b\pi\rho^2$. Thus the loop habit plane may tilt freely within the glide cylinder. The above parametrization may also be used to include tilting in the dipole-tensor approximation [35], though for carrying out a dynamic simulation one would also need an approximate analytic expression for the self-energy of a mixed ellipsoidal loop. Some expressions suitable for this purpose are already available in literature [68,69], but they are relatively limited in comparison with the general case addressed here.

The total potential energy of interacting loops is computed using the nonsingular de Wit formula [39], including the core energy (3). The energy has multiple stationary points at a given separation s, which are not trivially identified. Here the total energy was minimized over tilt amplitudes of both loops $\{u^{(1)}, v^{(1)}, u^{(2)}, v^{(2)}\}$ using the BFGS [70] implementation in SciPy [71] for a broad range of initial tilt configurations. While this approach does not consistently identify all the stationary points, it still gives a qualitative overview of the potential energy landscape.

All the energy minima identified in this way are shown in Fig. 6. Multiple potential energy branches belonging to distinct tilt configurations are found. Note that transitions at a crossing may involve a significant change in tilting, and thus would involve a transition over a large energy barrier.

APPENDIX C: LANGEVIN EQUATION OF MOTION FOR THE LOOP-LOOP SEPARATION

Assuming that the relaxation of internal loop degrees of freedom occurs on a much shorter timescale than the COP diffusion, the adiabatic equation of motion for the individual loop COP is derived from the two equations of motion for the loops:

$$\begin{aligned} B\dot{z}_{\mathrm{COP}}^{(1)} &= -\frac{1}{L^{(1)}}\frac{\partial V(s)}{\partial z_{\mathrm{COP}}^{(1)}} + F_s^{(1)}, \\ B\dot{z}_{\mathrm{COP}}^{(2)} &= -\frac{1}{L^{(2)}}\frac{\partial V(s)}{\partial z_{\mathrm{COP}}^{(2)}} + F_s^{(2)}, \end{aligned} \tag{C1}$$

where $V \in V_S$ is a branch of the PES, and the total stochastic force $F_s^{(i)}$ with strength $\sigma_{\mathrm{COP}}^{(i)}$ acting on loop i is derived following Sec. II using

$$\left\langle F_s^{(i)}(t)F_s^{(i)}(t')\right\rangle = \frac{\sigma_s^2}{L^{(i)}}\delta(t-t'), \tag{C2}$$

leading to $\sigma_{\mathrm{COP}}^{(i)} = \sigma_s/\sqrt{L^{(i)}}$. The total energy derivative is evaluated using the chain rule with $s = z_{\mathrm{COP}}^{(2)} - z_{\mathrm{COP}}^{(1)}$, and the two equations of motion (C1) are subtracted, resulting in

$$B\dot{s} = -V'(s)\left(\frac{1}{L^{(2)}} + \frac{1}{L^{(1)}}\right) + F_s^{(2)} - F_s^{(1)}. \tag{C3}$$

The equation of motion (C3) simplifies further for the case $L^{(1)} = L^{(2)} = L$:

$$BL\dot{s} = -2V'(s) + F_s, \tag{C4}$$

where F_s is the net stochastic force with standard deviation $\sigma = \sigma_s\sqrt{2L}$, following the sum theorem of Gaussian distributed variables. Note that the expectation value of the loop velocity over independent trajectories is temperature independent as the stochastic force has zero mean:

$$\langle \dot{s} \rangle = -\frac{2}{BL} V'(s). \tag{C5}$$

[1] S. L. Dudarev, M. R. Gilbert, K. Arakawa, H. Mori, Z. Yao, M. L. Jenkins, and P. M. Derlet, Langevin model for real-time Brownian dynamics of interacting nanodefects in irradiated metals, Phys. Rev. B **81**, 224107 (2010).

[2] R. S. Barnes, The migration of large clusters of point defects in irradiated materials, J. Phys. Soc. Jpn. **18** (Suppl. III), 305 (1963).

[3] K. Arakawa, K. Ono, M. Isshiki, K. Mimura, M. Uchikoshi, and H. Mori, Observation of the one-dimensional diffusion of nanometer-sized dislocation loops, Science **318**, 956 (2007).

[4] S. J. Zinkle and B. N. Singh, Microstructure of neutron-irradiated iron before and after tensile deformation, J. Nucl. Mater. **351**, 269 (2006).

[5] M. L. Jenkins, Z. Yao, M. Hernández-Mayoral, and M. A. Kirk, Dynamic observations of heavy-ion damage in Fe and Fe-Cr alloys, J. Nucl. Mater. **389**, 197 (2009).

[6] Z. Yao, M. Hernández-Mayoral, M. L. Jenkins, and M. A. Kirk, Heavy-ion irradiations of Fe and Fe-Cr model alloys. Part 1: Damage evolution in thin-foils at lower doses, Philos. Mag. **88**, 2851 (2008).

[7] M. Hernández-Mayoral, Z. Yao, M. L. Jenkins, and M. A. Kirk, Heavy-ion irradiations of Fe and Fe-Cr model alloys. Part 2: Damage evolution in thin-foils at higher doses, Philos. Mag. **88**, 2881 (2008).

[8] K. Arakawa, T. Amino, and H. Mori, Direct observation of the coalescence process between nanoscale dislocation loops with different Burgers vectors, Acta Mater. **59**, 141 (2011).

[9] S. L. Dudarev, K. Arakawa, X. Yi, Z. Yao, M. L. Jenkins, M. R. Gilbert, and P. M. Derlet, Spatial ordering of nano-dislocation loops in ion-irradiated materials, J. Nucl. Mater. **455**, 16 (2014).

[10] B. D. Wirth, G. R. Odette, D. Maroudas, and G. E. Lucas, Energetics of formation and migration of self-interstitials and self-interstitial clusters in α-iron, J. Nucl. Mater. **244**, 185 (1997).

[11] Y. N. Osetsky, D. J. Bacon, and A. Serra, Thermally activated glide of small dislocation loops in metals, Philos. Mag. Lett. **79**, 273 (1999).

[12] Y. N. Osetsky, D. J. Bacon, A. Serra, B. N. Singh, and S. I. Golubov, One-dimensional atomic transport by clusters of self-interstitial atoms in iron and copper, Philos. Mag. **83**, 61 (2003).

[13] S. L. Dudarev, The non-Arrhenius migration of interstitial defects in bcc transition metals, C. R. Phys. **9**, 409 (2008).

[14] T. D. Swinburne, K. Arakawa, H. Mori, H. Yasuda, M. Isshiki, K. Mimura, M. Uchikoshi, and S. L. Dudarev, Fast, vacancy-free climb of prismatic dislocation loops in bcc metals, Sci. Rep. **6**, 30596 (2016).

[15] B. D. Wirth, G. R. Odette, D. Maroudas, and G. E. Lucas, Dislocation loop structure, energy and mobility of self-interstitial atom clusters in bcc iron, J. Nucl. Mater. **276**, 33 (2000).

[16] J. Marian, B. D. Wirth, A. Caro, B. Sadigh, G. R. Odette, J. M. Perlado, and T. Diaz de la Rubia, Dynamics of self-interstitial cluster migration in pure α-Fe and Fe-Cu alloys, Phys. Rev. B **65**, 144102 (2002).

[17] N. Anento, A. Serra, and Y. N. Osetsky, Atomistic study of multimechanism diffusion by self-interstitial defects in α-Fe, Model. Simul. Mater. Sci. Eng. **18**, 025008 (2010).

[18] P. M. Derlet, M. R. Gilbert, and S. L. Dudarev, Simulating dislocation loop internal dynamics and collective diffusion using stochastic differential equations, Phys. Rev. B **84**, 134109 (2011).

[19] C. Domain and C. S. Becquart, Solute-$\langle 111 \rangle$ interstitial loop interaction in α-Fe: A DFT study, J. Nucl. Mater. **499**, 582 (2018).

[20] H. Xu, Y. N. Osetsky, and R. E. Stoller, Self-evolving atomistic kinetic Monte Carlo: Fundamentals and applications, J. Phys.: Condens. Matter **24**, 375402 (2012).

[21] D. R. Mason, X. Yi, M. A. Kirk, and S. L. Dudarev, Elastic trapping of dislocation loops in cascades in ion-irradiated tungsten foils, J. Phys.: Condens. Matter **26**, 375701 (2014).

[22] L. K. Béland, Y. N. Osetsky, R. E. Stoller, and H. Xu, Interstitial loop transformations in FeCr, J. Alloys Compd. **640**, 219 (2015).

[23] L. K. Béland, Y. N. Osetsky, R. E. Stoller, and H. Xu, Kinetic activation–relaxation technique and self-evolving atomistic kinetic Monte Carlo: Comparison of on-the-fly kinetic Monte Carlo algorithms, Comput. Mater. Sci. **100**, 124 (2015).

[24] G. Po, Y. Cui, D. Rivera, D. Cereceda, T. D. Swinburne, J. Marian, and N. Ghoniem, A phenomenological dislocation mobility law for bcc metals, Acta Mater. **119**, 123 (2016).

[25] S. P. Fitzgerald, Kink pair production and dislocation motion, Sci. Rep. **6**, 39708 (2016).

[26] B. A. Szajewski, A. Hunter, and I. J. Beyerlein, The core structure and recombination energy of a copper screw dislocation: A Peierls study, Philos. Mag. **97**, 2143 (2017).

[27] B. Gurrutxaga-Lerma and J. Verschueren, Elastic models of dislocations based on atomistic Kanzaki forces, Phys. Rev. B **98**, 134104 (2018).

[28] M. Boleininger, T. D. Swinburne, and S. L. Dudarev, Atomistic-to-continuum description of edge dislocation core: Unification of the Peierls-Nabarro model with linear elasticity, Phys. Rev. Mater. **2**, 083803 (2018).

[29] P. A. Geslin and D. Rodney, Thermal fluctuations of dislocations reveal the interplay between their core energy and long-range elasticity, Phys. Rev. B **98**, 174115 (2018).

[30] Y. Zhang and A. H. W. Ngan, Dislocation-density dynamics for modeling the cores and Peierls stress of curved dislocations, Int. J. Plast. **104**, 1 (2018).

[31] G. Po, M. Lazar, N. C. Admal, and N. Ghoniem, A non-singular theory of dislocations in anisotropic crystals, Int. J. Plast. **103**, 1 (2018).

[32] D. N. Blaschke, Properties of dislocation drag from phonon wind at ambient conditions, Materials **12**, 948 (2019).

[33] M. Hiratani and H. M. Zbib, Stochastic dislocation dynamics for dislocation-defects interaction: A multiscale modeling approach, J. Eng. Mater. Technol. **124**, 335 (2002).

[34] M. Hiratani and H. M. Zbib, On dislocation–defect interactions and patterning: Stochastic discrete dislocation dynamics (SDD), J. Nucl. Mater. **323**, 290 (2003).

[35] S. L. Dudarev and A. P. Sutton, Elastic interactions between nano-scale defects in irradiated materials, Acta Mater. **125**, 425 (2017).

[36] S. L. Dudarev and P. W. Ma, Elastic fields, dipole tensors, and interaction between self-interstitial atom defects in bcc transition metals, Phys. Rev. Mater. **2**, 033602 (2018).

[37] X. Yi, A. E. Sand, D. R. Mason, M. A. Kirk, S. G. Roberts, K. Nordlund, and S. L. Dudarev, Direct observation of size scaling and elastic interaction between nano-scale defects in collision cascades, Europhys. Lett. **110**, 36001 (2015).

[38] J. Drouet, L. Dupuy, F. Onimus, F. Mompiou, S. Perusin, and A. Ambard, Dislocation dynamics simulations of interactions between gliding dislocations and radiation induced prismatic loops in zirconium, J. Nucl. Mater. **449**, 252 (2014).

[39] W. Cai, A. Arsenlis, C. R. Weinberger, and V. V. Bulatov, A non-singular continuum theory of dislocations, J. Mech. Phys. Solids **54**, 561 (2006).

[40] V. V. Bulatov and W. Cai, *Computer Simulations of Dislocations* (Oxford University Press, Oxford, 2006), Vol. 3.

[41] B. A. Szajewski, F. Pavia, and W. A. Curtin, Robust atomistic calculation of dislocation line tension, Model. Simul. Mater. Sci. Eng. **23**, 085008 (2015).

[42] L. Dupuy and M. C. Fivel, A study of dislocation junctions in fcc metals by an orientation dependent line tension model, Acta Mater. **50**, 4873 (2002).

[43] H. L. Pécseli, *Fluctuations in Physical Systems* (Cambridge University Press, Cambridge, England, 2000), p. 74.

[44] R. Kubo, The fluctuation-dissipation theorem, Rep. Prog. Phys. **29**, 255 (1966).

[45] T. D. Swinburne, S. L. Dudarev, and A. P. Sutton, Classical Mobility of Highly Mobile Crystal Defects, Phys. Rev. Lett. **113**, 215501 (2014).

[46] T. D. Swinburne and S. L. Dudarev, Phonon drag force acting on a mobile crystal defect: Full treatment of discreteness and nonlinearity, Phys. Rev. B **92**, 134302 (2015).

[47] K. Ohsawa and E. Kuramoto, Thermally activated transport of a dislocation loop within an elastic model, J. Nucl. Mater. **367–370**, 327 (2007).

[48] T. D. Swinburne, Collective transport in the discrete Frenkel-Kontorova model, Phys. Rev. E **88**, 012135 (2013).

[49] L. Proville, D. Rodney, and M. Marinica, Quantum effect on thermally activated glide of dislocations, Nat. Mater. **11**, 845 (2012).

[50] T. D. Swinburne, P. W. Ma, and S. L. Dudarev, Low temperature diffusivity of self-interstitial defects in tungsten, New J. Phys. **19**, 073024 (2017).

[51] X. J. Shi, L. Dupuy, B. Devincre, D. Terentyev, and L. Vincent, Interaction of ⟨100⟩ dislocation loops with dislocations studied by dislocation dynamics in α-iron, J. Nucl. Mater. **460**, 37 (2015).

[52] Y. Li, C. Robertson, M. Shukeir, and L. Dupuy, Screw dislocation interaction with irradiation defect-loops in α-iron: Evaluation of cross-slip effect using dislocation dynamics simulations, Model. Simul. Mater. Sci. Eng. **26**, 055009 (2018).

[53] R. O. Scattergood and D. J. Bacon, The Orowan mechanism in anisotropic crystals, Philos. Mag. **31**, 179 (1975).

[54] X. Han, N. M. Ghoniem, and Z. Wang, Parametric dislocation dynamics of anisotropic crystals, Philos. Mag. **83**, 3705 (2003).

[55] J. Yin, D. M. Barnett, and W. Cai, Efficient computation of forces on dislocation segments in anisotropic elasticity, Model. Simul. Mater. Sci. Eng. **18**, 045013 (2010).

[56] S. P. Fitzgerald and S. Aubry, Self-force on dislocation segments in anisotropic crystals, J. Phys.: Condens. Matter **22**, 295403 (2010).

[57] G. J. Ackland, M. I. Mendelev, D. J. Srolovitz, S. Han, and A. V. Barashev, Development of an interatomic potential for phosphorus impurities in α-iron, J. Phys.: Condens. Matter **16**, S2629 (2004).

[58] X. Shi, Etude par simulations de dynamique des dislocations des effets d'irradiation sur la ferrite à haute température, Ph.D. thesis, Université Pierre et Marie Curie-Paris VI, 2014.

[59] L. D. Landau and E. M. Lifshitz, *Theory of Elasticity* (Pergamon, Oxford, England, 1970), p. 127.

[60] K. Kang, V. V. Bulatov, and W. Cai, Singular orientations and faceted motion of dislocations in body-centered cubic crystals, Proc. Natl. Acad. Sci. **109**, 15174 (2012).

[61] P. M. Anderson, J. P. Hirth, and J. Lothe, *Theory of Dislocations* (Cambridge University Press, Cambridge, 2017).

[62] E. Clouet, C. Varvenne, and T. Jourdan, Elastic modeling of point-defects and their interaction, Comput. Mater. Sci. **147**, 49 (2018).

[63] C. A. Ullrich, *Time-Dependent Density Functional Theory* (Oxford University Press, Oxford, England, 2012), p. 11.

[64] A. J. E. Foreman and J. D. Eshelby, Elastic interaction energy of dislocation loops, Tech. Rep. AERE Report 4170, Atomic Energy Research Establishment, Harwell, England, 1962.

[65] H. Risken, *The Fokker-Planck Equation* (Springer, Berlin, 1996), pp. 63–95.

[66] V. I. Melnikov, The Kramers problem: Fifty years of development, Phys. Rep. **209**, 1 (1991).

[67] B. U. Felderhof, Diffusion and convection after escape from a potential well, Physica A **388**, 1388 (2009).

[68] W. G. Wolfer, T. Okita, and D. M. Barnett, Motion and Rotation of Small Glissile Dislocation Loops in Stress Fields, Phys. Rev. Lett. **92**, 085507 (2004).

[69] H. J. Chu, J. Wang, C. Z. Zhou, and I. J. Beyerlein, Self-energy of elliptical dislocation loops in anisotropic crystals and its application for defect-free core/shell nanowires, Acta Mater. **59**, 7114 (2011).

[70] J. Nocedal and S. J. Wright, *Numerical Optimization*, 2nd ed. (Springer, Berlin, 2006).

[71] E. Jones, E. Oliphant, P. Peterson *et al.*, SciPy: open source scientific tools for Python (2001-), http://www.scipy.org/ [online; accessed 2019-07-13].